Spiral vortices in compressible turbulent flows

T. Gomez, H. Politano, A. Pouquet, and M. Larchevêque

Citation: Physics of Fluids **13**, 2065 (2001); doi: 10.1063/1.1367368
View online: http://dx.doi.org/10.1063/1.1367368
View Table of Contents: http://scitation.aip.org/content/aip/journal/pof2/13/7?ver=pdfcov
Published by the AIP Publishing

Spiral vortices in compressible turbulent flows

T. Gomez[a)]
Laboratoire de Modélisation en Mécanique, CNRS UMR 7606, Université Paris VI, Jussieu, Paris Cedex 5, France

H. Politano
Observatoire de la Côte d'Azur, CNRS UMR 6529 BP 4229, 06304 Nice Cedex 4, France

A. Pouquet
NCAR, P.O. Box 3000, Boulder, Colorado 80307-3000

M. Larchevêque
Laboratoire de Modélisation en Mécanique, CNRS UMR 7606, Université Paris VI, Jussieu, Paris Cedex 5, France

(Received 23 June 2000; accepted 1 March 2001)

We extend the spiral vortex solution of Lundgren [Phys. Fluids **25**, 2193 (1982)] to compressible turbulent flows with a perfect gas. This model links the dynamical and the spectral properties of incompressible flows, providing a $k^{-5/3}$ Kolmogorov energy spectrum. In so doing, a compressible spatiotemporal transformation is derived, reducing the dynamics of three-dimensional vortices, stretched by an axisymmetric incompressible strain, into a two-dimensional compressible vortex dynamics. It enables us to write the three-dimensional spectra of the incompressible and compressible square velocities in terms of, respectively, the two-dimensional spectra of the enstrophy and of the square velocity divergence, by the use of a temporal integration. Numerical results are presented from decaying direct simulations performed with 512^2 grid points; initially, the rms Mach number is 0.23, with local values up to 0.9, the Reynolds number is 700, and the ratio between compressible and incompressible square velocities is 0.1. A $k^{-5/3}$ inertial behavior is seen to result from the dynamical evolution for both the compressible and incompressible three-dimensional spectra. © *2001 American Institute of Physics.* [DOI: 10.1063/1.1367368]

I. INTRODUCTION

To study turbulence through the dynamics of the small scale structures which develop and their spectral counterpart, Lundgren[1] introduced a model based on the intermittent fine scales of incompressible turbulent flows thought as consisting in a collection of uncorrelated stretched spiral vortices, randomly oriented in space and individually subject to an axisymmetric irrotational straining field produced by larger scales. The basic small scale structures are assumed to be created by large scale processes, excluded in the dynamics of the model, like Kelvin–Helmholtz instabilities or vortex interaction mechanisms. These processes would produce a given quantity N of vortex length per unit time and unit volume, constant for a stationary turbulence.

This model is actually the only one which provides analytically the famous $k^{-5/3}$ spectrum of Kolmogorov,[2] although this kind of approach had already been introduced in the Townsend model[3] dealing with randomly oriented Burgers vortices and leading to a k^{-1} spectrum (see the following).

The central point of these vortex-based models is the use of a spatial set of small scale structures, which are taken as local solutions of the Navier–Stokes equations. A few models using tube-like or sheet-like structures have been investigated as well by Corrsin[4] and Tennekes.[5] The basic solution has to contain the essential physics of the fine scale mechanism of balance between vorticity production, by the local strain rate, and vorticity dissipation, by viscosity.

The model due to Townsend predicts a k^{-1} scaling law for the energy spectrum in the case of the axisymmetric Burgers vortex and a k^{-2} law for the plane Burgers layer for small scales ($k \gg 1$), basically because of the singular nature of such structures. Obviously, the Kolmogorov exponent ($-5/3$) lies between the values obtained for the tube-like and sheet-like structures. This suggests that, in order to obtain the $k^{-5/3}$ scaling law, the vorticity field might be composed of a mixture of both structures. The properties of the axial straining combined with the roll-up of nonaxisymmetric vorticity structures give rise to the most interesting model, the so-called ''stretched spiral vortex'' proposed by Lundgren;[1] it produces rich physical properties both in the inertial and in the dissipative ranges.[6,7]

It can thus be expected that any Navier–Stokes solution which includes the roll-up of fine vorticity gradients in a strain field may produce a $k^{-5/3}$ scaling law as noted by Lundgren.[8] All these models have been sought considering incompressible Navier–Stokes dynamics. What happens in the compressible case? Porter *et al.*[9,10] performed numerical simulations at high resolution in three dimensions, for either decaying or forced compressible turbulent flows at a rms Mach number of unity, using the Piecewise Parabolic Method (or PPM algorithm).[11] They showed that, in compressible turbulence, the solenoidal velocity spectrum has a

a)Electronic mail: gomez@lmm.jussieu.fr

$k^{-5/3}$ scaling in the inertial range and, more surprisingly, that the compressible velocity spectrum has the same behavior. They also showed that the vorticity field organizes in strong filaments and weaker sheets and spirals,[12] whereas the shocks are mostly planar when they appear. Thus the purpose of this paper is to seek an explanation for such a behavior along the lines of the Lundgren vortex model.

In Sec. II, we extend the Lundgren spatiotemporal transformation to the dynamics of a compressible flow with perfect gas law. This transformation allows one to reduce the dynamics of a three-dimensional flow to that of a two-dimensional one. We then describe the three-dimensional velocity spectra obtained for compressible homogeneous turbulent flows by the use of a temporal integration of the two-dimensional spectra of the enstrophy and of its compressible counterpart: the square velocity divergence. In Sec. III, using direct numerical simulations in two space dimensions, we deduce the spectral properties of a three-dimensional stationary turbulent flow from the temporal evolution of the two-dimensional flow.[13] Section IV presents conclusions together with a discussion of the implications of these results.

II. THE COMPRESSIBLE LUNDGREN TRANSFORMATION

A. The incompressible model

For completeness, we first recall the essential steps of the Lundgren model[1] in the incompressible case. One first considers a vortex structure parallel to the z direction, say, and independent of the z variable: $(\omega_r,\omega_\theta,\omega_z,t)=(0,0,\omega(r,\theta,t))$, in the presence of an axisymmetric strain $(-a(t)r/2,0,a(t)z)$, modeling the effect of the large scales. By use of a spatiotemporal change of variables, the dynamics for the three-dimensional vorticity can be reduced to the dynamics of a two-dimensional flow. An asymptotic vorticity solution of the two-dimensional Navier–Stokes equations is then obtained at large time and small viscosity.[1] This solution, $\omega_2(\xi,\theta,\tau)$, describes the roll-up of a spiral of vorticity, with an arbitrary number of branches, by an axisymmetric central core. The solution is generic in the sense that the vorticity distribution along the branches can be set arbitrarily and it is consistent with the existence of an infinite number of conserved moments of the vorticity field for two-dimensional inviscid flows.

The unsteady evolution of the three-dimensional vorticity field reads

$$\omega(r,\theta,t)=e^{at}\omega_2(\xi,\theta,\tau), \tag{1}$$

$$\omega_2(\xi,\theta,\tau)=\sum_{n=-\infty}^{\infty}\omega_2^{(n)}(\xi,\tau)\exp(in\theta), \tag{2}$$

$$\omega_2^{(n)}(\xi,\tau)=f^{(n)}(\xi)\exp(-in\Omega(\xi)\tau-\nu n^2\Lambda^2(\xi)\tau^3/3), \tag{3}$$

$$\omega_2^{(0)}(\xi)=g(\xi)+f^{(0)}(\xi), \tag{4}$$

$$\xi(r,t)=re^{at/2}, \tag{5}$$

$$\tau(t)=\frac{e^{at}-1}{a}, \tag{6}$$

where

$$\frac{1}{\xi}\frac{d}{d\xi}(\xi^2\Omega(\xi))=g(\xi)+f^{(0)}(\xi), \tag{7}$$

and

$$\Lambda=\frac{d\Omega}{d\xi}. \tag{8}$$

The variables (ξ,τ) are the stretched variables in space and time, corresponding to a purely two-dimensional evolution, a is the uniform positive strain rate of the external field, ν is the kinematic viscosity, $e^{at}f^{(n)}(\xi)$ is the θ-averaged vorticity for the vortex, and $e^{at}g(\xi)$ describes the axisymmetric background vorticity field. The spiral property is given by $\Omega(\xi)$, a monotonous decreasing function with ξ, which gives the two-dimensional θ-averaged angular velocity.

This solution, which describes the dynamics of a stretched spiral vortex subject to a constant strain rate, is then used to calculate the velocity spectrum of three-dimensional homogeneous turbulence assuming several important hypotheses. Namely, in this ansatz, the local structures, which are taken as N randomly oriented vortices, are supposed to fill a box of size L at a time t; this means that each vortex can be represented by the state of a unique vortex at a given age. All the vortices present the same temporal evolution starting from times t_n, randomly shifted, and have the same length l_0 at times of creation. They do not interact between themselves and the vorticity lies along the axis of the tube, aligned with an eigenvector of the external strain (see Gibbon *et al.*[14] for a discussion on this latter point). Some external process creates these spiral vortices at a rate N_c per unit time, and destroy them when the spiral branches have been dissipated. Thus a statistical equilibrium is maintained with a constant number of structures.

Furthermore, an ergodic hypothesis is introduced, summed up here as

$$\sum_{n=1}^{n=N}[\cdots]=N_c\int_{t_1}^{t_2}[\cdots]dt, \tag{9}$$

where $[\cdots]$ is any physical quantity of the model, like the velocity spectrum, where t_1 is the creation time and t_2 the destruction time of the spiral component of the local vorticity structure. The physical interpretation of this strong hypothesis is that the ensemble average over all uncorrelated vortices in a stationary developed turbulence, with different ages, can be replaced by a temporal integration over the history of a unique vortex.

The energy spectrum $E(k)$ is computed from the enstrophy spectrum $E_{\omega\omega}(k)$, namely $E(k)=E_{\omega\omega}(k)/2k^2$. The three-dimensional enstrophy spectrum is itself evaluated from the two-dimensional vorticity using the spatiotemporal transformation and the previous ergodic hypothesis. The shell-summed velocity spectrum of the ensemble is

$$E(k)=E_0(k)+\frac{4\pi}{3}Na^{1/3}k^{-5/3}\times\exp\left[-\frac{2\nu k^2}{3a}\right]\sum_{n=1}^{n=\infty}n^{-4/3}\int_0^\infty\frac{|f_n(\xi)|^2}{|\Lambda(\xi)|^{4/3}}\xi\,d\xi, \tag{10}$$

where $N=N_c l_0/L^3$. $E_0(k)$ is the spectral component coming from the axisymmetric term [Eq. (4)], and the second term is the contribution of the nonaxisymmetric terms $n\neq 0$ [Eq. (3)].

The second term on the right-hand side of Eq. (10) dominates E_0 at small wave numbers and thus a $k^{-5/3}$ scaling law is obtained[1] in the inertial range when $k(\nu/a)^{1/2}\ll 1$. This result is derived using the two-dimensional analytical solution with constant strain rate a assumed to be provided by larger scales. Lundgren[8] showed using numerical considerations that the spectral index is not considerably influenced by taking a time-dependent strain rate, and this assumption is largely used by different authors in the literature.

B. The compressible transformation and solutions

Similar to the Lundgren solution, we consider a problem in which the fluid is strained by an axisymmetric flow of the form

$$\mathbf{u}_{\text{strain}}=(-a(t)r/2,0,a(t)z) \tag{11}$$

with $\boldsymbol{\nabla}\cdot(\mathbf{u}_{\text{strain}})=0$ and where $a(t)$ is the strain rate. We are looking for a solution in which there is only a z component of vorticity, with all the variables independent of z. The compressible Navier–Stokes equations for the vorticity $\boldsymbol{\omega}=\boldsymbol{\nabla}\times\mathbf{u}=(0,0,\omega)$ and the velocity divergence $d=\boldsymbol{\nabla}\cdot\mathbf{u}$ with a constant dynamic viscosity μ can be written as

$$\frac{\partial\rho}{\partial t}+(\mathbf{u}+\mathbf{u}_{\text{strain}})\cdot\boldsymbol{\nabla}\rho=-\rho d, \tag{12}$$

$$\frac{\partial\omega}{\partial t}+(\mathbf{u}+\mathbf{u}_{\text{strain}})\cdot\boldsymbol{\nabla}\omega=a(t)\omega-\omega d+\frac{1}{\rho^2}(\boldsymbol{\nabla}\rho\times\boldsymbol{\nabla}p)+\frac{\mu}{\rho}(\nabla^2\omega)+\mu\boldsymbol{\nabla}\left(\frac{1}{\rho}\right)\times\left[-\boldsymbol{\nabla}\times\boldsymbol{\omega}+\frac{4}{3}\boldsymbol{\nabla}d\right], \tag{13}$$

$$\frac{\partial d}{\partial t}+(\mathbf{u}+\mathbf{u}_{\text{strain}})\cdot\boldsymbol{\nabla}d=a(t)d-\boldsymbol{\nabla}\mathbf{u}:\boldsymbol{\nabla}\mathbf{u}-\frac{3}{2}a^2(t)-\frac{1}{\rho}\nabla^2p+\frac{1}{\rho^2}\boldsymbol{\nabla}\rho\cdot\boldsymbol{\nabla}p+\frac{4}{3}\frac{\mu}{\rho}\nabla^2d+\mu\boldsymbol{\nabla}\left(\frac{1}{\rho}\right)\cdot\left[-\boldsymbol{\nabla}\times\boldsymbol{\omega}+\frac{4}{3}\boldsymbol{\nabla}d\right], \tag{14}$$

$$\frac{\partial e}{\partial t}+(\mathbf{u}+\mathbf{u}_{\text{strain}})\cdot\boldsymbol{\nabla}e=-(\gamma-1)ed+\frac{\mu}{\rho}\left(\boldsymbol{\tau}:\mathbf{D}-ad+\frac{3}{2}a(t)^2\right)+\frac{\kappa}{\rho}\nabla^2T, \tag{15}$$

where ρ is the mass density and e the internal energy per unit mass. The temperature T is related to the internal energy e by the relation $e=C_vT$, assuming constant specific heats C_v and C_p. Let us then add the perfect gas law

$$\frac{p}{\rho}=RT, \tag{16}$$

where R is the specific gas constant. The viscous stress tensor is defined as $\tau_{ij}=-2/3\boldsymbol{\nabla}\cdot\mathbf{u}\delta_{ij}+2D_{ij}$, where δ_{ij} is the Kronecker symbol and the strain tensor is defined as $D_{ij}=1/2(\partial_j u_i+\partial_i u_j)$. These equations conserve mass, momentum, and total energy.

Note that in Eq. (14) for the velocity divergence, there is a term of divergence production by the strain, $a(t)d$, similar to the term of vorticity production in Eq. (13) for the vorticity.

In order to reduce the three-dimensional dynamics to a two-dimensional one, the change of variables in space and time is defined, similarly to the incompressible case, as

$$S(t)=\exp\int_0^t a(t')dt', \tag{17}$$

$$\xi(t)=S^{1/2}(t)\tau, \tag{18}$$

$$\tau(t)=\int_0^t S(t')dt', \tag{19}$$

and, in the compressible case, the spatiotemporal transformations between the three- and two-dimensional fields and thermodynamic variables take the form

$$\omega(r,\theta,t)=S(t)\omega_2(\xi,\theta,\tau), \tag{20}$$

$$d(r,\theta,t)=S(t)d_2(\xi,\theta,\tau), \tag{21}$$

$$\mathbf{u}(r,\theta,t)=S^{1/2}(t)\mathbf{u}_2(\xi,\theta,\tau), \tag{22}$$

$$\rho(r,\theta,t)=\rho_2(\xi,\theta,\tau), \tag{23}$$

$$e(r,\theta,t)=S(t)e_2(\xi,\theta,\tau), \tag{24}$$

$$p(r,\theta,t)=S(t)p_2(\xi,\theta,\tau), \tag{25}$$

where the subscript 2 denotes the two-dimensional flow.

The behavior of the compressible velocity spectrum of the vortex structures, which describe the local dynamics of turbulent flows, can be investigated under the two following assumptions. First, there exists a scale separation between the large scales of the external strain and the internal fluctuations of the vortex structures at scales comparable to their cross-sectional diameters. Thus, we assume that the internal fluctuations in planes perpendicular to the local structures are provided only by the velocity field of the structures themselves. A similar hypothesis has been introduced by Pullin[15] to evaluate the pressure spectrum of the incompressible

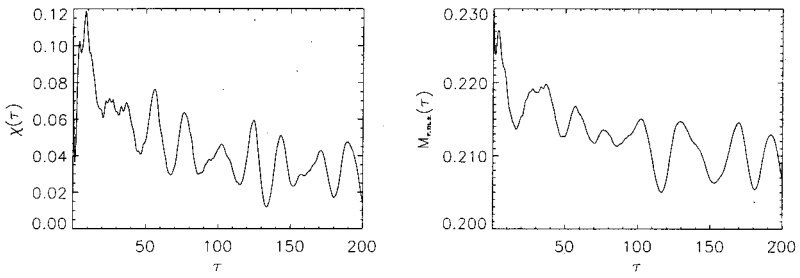

FIG. 1. Temporal evolution of the ratio $\chi(\tau)=E^d(\tau)/E^s(\tau)$ at left; and of the rms Mach number $M_{\rm rms}(\tau)$ at right.

Lundgren vortex. Second, the dynamical solutions are considered for large rescaled time τ and small viscosity.

Under these assumptions, the spatiotemporal transformation enables us to find solutions of Eqs. (12)–(15) based on the solutions of the transformed equations which correspond to the dynamics of a purely two-dimensional flow. When transforming the three-dimensional equations, using Eqs. (17)–(25), the nonlinear terms, proportional to a^2, resulting from the self-interaction of the large scales of the external strain field are neglected in the two-dimensional dynamics of the local structure, as well as a term of order $1/\tau$ on the right-hand side of the equation of the internal energy, as we are looking for solutions at large τ. Starting from the three-dimensional dynamics, we obtain the following set of equations involving the two-dimensional fields in the rescaled time and space variables:

$$\frac{\partial \rho_2}{\partial \tau}+\mathbf{u}_2\cdot\boldsymbol{\nabla}_\xi\rho_2=-\rho d_2, \tag{26}$$

$$\frac{\partial \omega_2}{\partial \tau}+\mathbf{u}_2\cdot\boldsymbol{\nabla}_\xi\omega_2=-\omega_2 d_2+\frac{1}{\rho_2^2}(\boldsymbol{\nabla}_\xi\rho_2\times\boldsymbol{\nabla}_\xi p_2)+\frac{\mu}{\rho_2}(\nabla_\xi^2\omega_2)+\mu\boldsymbol{\nabla}_\xi\left(\frac{1}{\rho_2}\right)\times\left[-\boldsymbol{\nabla}_\xi\times\omega_2+\frac{4}{3}\boldsymbol{\nabla}_\xi d_2\right], \tag{27}$$

$$\frac{\partial d_2}{\partial \tau}+\mathbf{u}_2\cdot\boldsymbol{\nabla}_\xi d_2=-\boldsymbol{\nabla}_\xi u_2:\boldsymbol{\nabla}_\xi\mathbf{u}_2-\frac{1}{\rho_2}\nabla_\xi^2 p_2+\frac{1}{\rho_2^2}\boldsymbol{\nabla}_\xi\rho_2\cdot\boldsymbol{\nabla}_\xi p_2+\frac{4}{3}\frac{\mu}{\rho_2}\nabla_\xi^2 d_2+\mu\boldsymbol{\nabla}_\xi\left(\frac{1}{\rho_2}\right)\cdot\left[-\boldsymbol{\nabla}_\xi\times\omega_2+\frac{4}{3}\boldsymbol{\nabla}_\xi d_2\right], \tag{28}$$

$$\frac{\partial e_2}{\partial \tau}+\mathbf{u}_2\cdot\boldsymbol{\nabla}_\xi e_2+(\gamma-1)e_2 d_2-\frac{\mu}{\rho_2}(\boldsymbol{\tau}_2:\mathbf{D}_2)-\frac{\kappa}{\rho_2}\nabla_\xi^2 T_2=-\frac{a}{S(\tau)}\left(e_2+\frac{\mu}{\rho_2}d_2\right) \tag{29}$$

with the perfect gas law

$$\frac{p_2}{\rho_2}=RT_2, \tag{30}$$

where $\boldsymbol{\nabla}_\xi$ denotes the gradient in the stretched variables. A supplementary simplifying assumption is to discard the right-hand side of the internal energy equation (29): the $1/S(\tau)$ coefficient, of order $1/\tau$, is likely to render those terms small compared to the left-hand side of the equation, since, in the spirit of the Lundgren analysis, the temporal integration is carried out for long rescaled times ($\tau\sim 50-200$).[8] In the context of the incompressible Lundgren model, an analytic solution can be found, as recalled in Sec. II, and the Kolmogorov spectrum emerges from an integration over time using the approximation of the stationary phase. In the compressible case, in view of the obvious complexity of the equivalent model coupling all variables, we shall seek here a numerical approach to be given in the next section. However, the definition of the velocity spectrum is first introduced.

C. The compressible velocity spectrum

The velocity is decomposed as usual into two parts

$$\mathbf{u}=\mathbf{u}^s+\mathbf{u}^d, \tag{31}$$

where

$$\boldsymbol{\nabla}\times\mathbf{u}^d=0,\quad \boldsymbol{\nabla}\cdot\mathbf{u}^s=0; \tag{32}$$

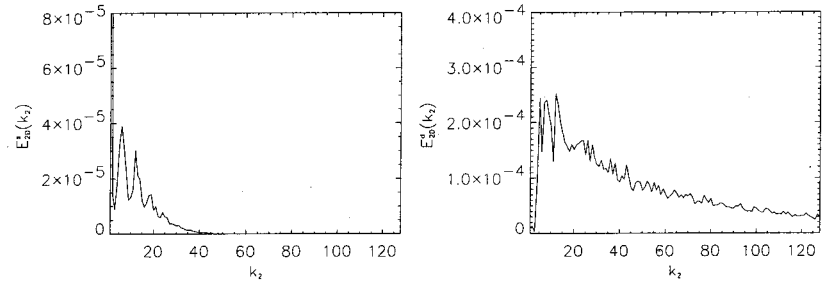

FIG. 2. Two-dimensional spectra at time $\tau=30$: for the incompressible square velocity $E^s(k)$ at left, and for the compressible square velocity divergence $E^d(k)$ at right.

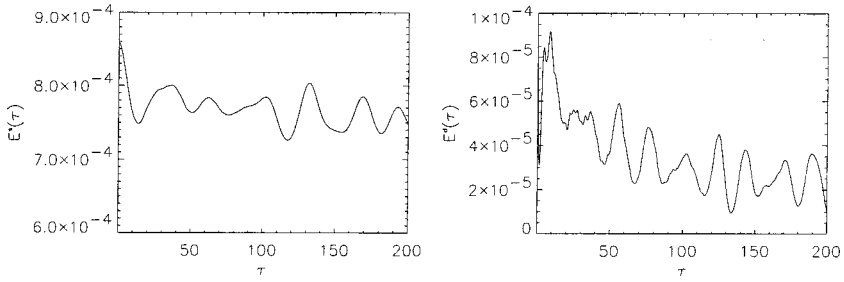

FIG. 3. Temporal evolution of the incompressible square velocity $E^s(\tau)$ at left, of the compressible square velocity $E^d(\tau)$ at right.

$\mathbf{u}^s$ is the solenoidal velocity and $\mathbf{u}^d$ the dilatational velocity. The velocity decomposition (31) led Moyal[16] to introduce the decomposed spectra

$$E(k)=E^s(k)+E^d(k), \tag{33}$$

where

$$E^s(k)=\int\int \hat{\mathbf{u}}^s\cdot\hat{\mathbf{u}}^{s*}dS_k, \tag{34}$$

and

$$E^d(k)=\int\int \hat{\mathbf{u}}^d\cdot\hat{\mathbf{u}}^{d*}dS_k, \tag{35}$$

where an asterisk denotes complex conjugates and $\hat{\mathbf{u}}$ the Fourier transform of the velocity.

The method developed by Lundgren[8] to obtain the three-dimensional kinetic energy spectrum of an incompressible flow from two-dimensional numerical simulations consists in a time integration of the two-dimensional square vorticity (enstrophy) spectrum. In the compressible case, we can define the corresponding physical quantities, with the added ingredient of the velocity divergence $d=\boldsymbol{\nabla}\cdot\mathbf{u}$.

The power spectrum of the velocity divergence can be written in terms of the Fourier integral of the velocity divergence correlation function

$$R_{dd}(\boldsymbol{\rho},t)=\frac{1}{L^3}\int d(\mathbf{r},t)\cdot d(\mathbf{r}+\boldsymbol{\rho},t)\mathbf{dr}, \tag{36}$$

where L is the length of the box, and of its Fourier transformation

$$\Phi_{dd}(\mathbf{k},t)=\frac{1}{2\pi^3}\int_{\text{all }\boldsymbol{\rho}}\exp(-i\mathbf{k}\cdot\boldsymbol{\rho})R_{dd}(\boldsymbol{\rho},t)\mathbf{d}\boldsymbol{\rho}. \tag{37}$$

In the case of three-dimensional compressible homogeneous turbulence, the compressible velocity spectrum is

$$E^d(k,t)=F(k,t)/2k^2 \tag{38}$$

with F the velocity divergence spectrum obtained by integration in spherical shells S_k of radius k in wave number space

$$F(k,t)=\int \Phi_{dd}(\mathbf{k},t)dS_k. \tag{39}$$

If we consider a stationary turbulence, and assume that the velocity divergence is concentrated in the vicinity of the vortex filaments which are themselves isolated and created at a constant rate N_c, with the same structure and the same strength, we can invoke the ergodic hypothesis as in Lundgren to transform a space integration into a time integration on the temporal evolution of a single structure. The compressible velocity spectrum is thus expressed as

$$E^d(k)=\frac{2\pi^2N_c}{L^3}\frac{1}{k^2}\int_0^{\tau_{\text{cut}}}l(\tau)F(k,\tau)d\tau, \tag{40}$$

where τ_{cut} is the lifetime of the spiral structure and $l(\tau)$ the filament length.

III. NUMERICAL EXPERIMENTS

A. Numerical setup

We consider a medium of characteristic length L, of mean density ρ_0, and mean velocity u_0. These quantities are used to normalize to unity the density ρ and the velocity $\mathbf{u}$, and the spatial scale (size of the computational box) is 2π. The internal energy is normalized by u_0^2 and is related to the temperature as usual by $e=C_vT$ with the nondimensionalized constant parameter $C_v=1/(\gamma(\gamma-1))M_0^2$; the initial Mach number is $M_0=u_0/c_0$ where the speed of sound is defined as $c_0^2=\gamma RT_0$ with γ the adiabatic index and R the perfect-gas constant. The normalization temperature T_0 on which the sound velocity is based, is set to ensure that the

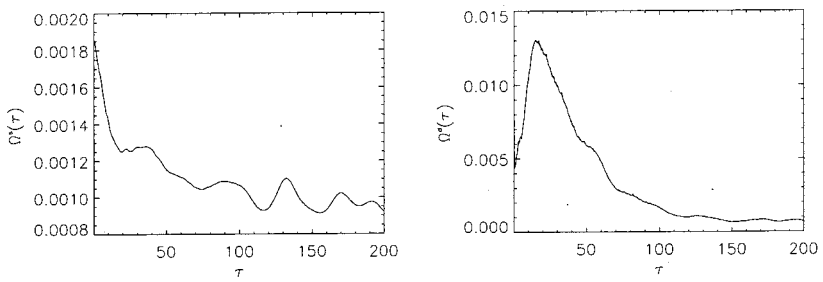

FIG. 4. Temporal evolution of enstrophy $\Omega^s(\tau)$ at left, and of its compressible counterpart $\Omega^d(\tau)=\frac{1}{2}\langle(\boldsymbol{\nabla}\cdot\mathbf{u})^2\rangle$ at right.

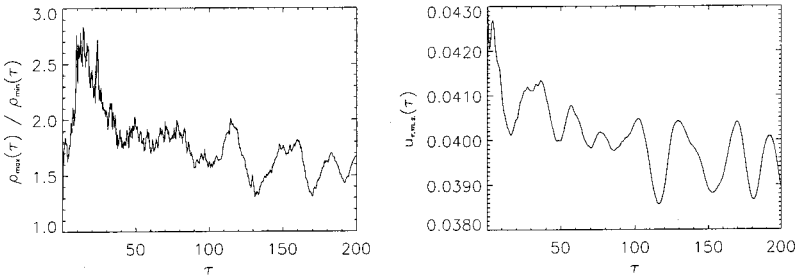

FIG. 5. Temporal evolution of the ratio of the maximum to the minimum of the mass density $\rho_{max}(\tau)/\rho_{min}(\tau)$ at left, and temporal evolution of the rms velocity at right.

temperature variable is of order unity. Furthermore, we take the eddy turnover time L/u_0 as the dependent unit. In the code, the equations for conservation of mass, momentum, and internal energy are written in the following nondimensionalized form:

$$\frac{\partial \rho}{\partial t} + \mathbf{u}\cdot\nabla\rho = -\rho\nabla\cdot\mathbf{u}, \tag{41}$$

$$\frac{\partial \mathbf{u}}{\partial t} + \mathbf{u}\cdot\nabla\mathbf{u} = -\frac{1}{\rho}\nabla p + \frac{1}{\rho\,\mathrm{Re}}\left(\nabla^2\mathbf{u} + \frac{1}{3}\nabla(\nabla\cdot\mathbf{u})\right), \tag{42}$$

$$\frac{\partial e}{\partial t} + \mathbf{u}\cdot\nabla e = -(\gamma-1)e\nabla\cdot\mathbf{u} + \frac{1}{\rho\,\mathrm{Re}}(\boldsymbol{\tau}:\mathbf{D}) + \frac{\gamma}{\mathrm{Pr}\,\mathrm{Re}}\nabla^2 T, \tag{43}$$

where ρ is the mass density, $\mathbf{u}$ the velocity, and e the internal energy per unit mass; $\boldsymbol{\tau}$ and $\mathbf{D}$ are, respectively, the stress tensor and the strain tensor defined as in Sec. II B. The two dimensionless parameters that arise are the Reynolds number $\mathrm{Re}=\rho_0 u_0 L_0/\mu$ and the Prandtl number $\mathrm{Pr}=\mu C_p/\kappa=\nu/\eta$ where κ is the constant thermal conductivity, ν the kinematic viscosity, and η the thermal diffusivity. The perfect gas law in nondimensional form writes $p=(\gamma-1)\rho e$.

Using periodic boundary conditions with a Fourier representation, the numerical simulations are performed with a pseudospectral code. The temporal scheme is a third-order Runge–Kutta scheme, the intermediate steps of which rely on an Euler scheme for the nonlinear terms and a Cranck–Nicholson scheme for the dissipative ones. The wave numbers vary from $k_{min}=1$ to $k_{max}=\mathcal{N}/2$, where $\mathcal{N}$ is the number of grid points in each direction, with $\mathcal{N}$ up to 512.

B. Initial conditions

As stated before, the velocity fluctuations can be uniquely distributed via the Helmholtz decomposition into a solenoidal part whose Fourier transform is orthogonal to the wave vector $\mathbf{k}$, and a dilatational part with its Fourier transform collinear to $\mathbf{k}$.[16] The incompressible part of the initial velocity distribution is given by the Lundgren spiral solution at a given nondimensional time.[8] The compressible part of the velocity is taken as a Gaussian noise with an energy spectrum at small scales analogous to the incompressible part, and set up at wave numbers corresponding to the branches of the spiral in a range excluding essentially the five first modes linked to the vortex core. This is done in order to favor the interactions between the compressible and spiral incompressible components of the velocity field. This condition allows for an intensification of the interactions between incompressible and compressible modes. The total compressible kinetic energy level is given through the ratio $\chi=E^d/E^s$, initially equal to 0.1 in the simulations. Note that χ is a second free parameter, besides the Mach number, in compressible flows; the value chosen here is in keeping with most numerical simulations of supersonic flows, although high values of χ can arise in the context of the interstellar medium when energy is injected through supernovæ blast waves or through heating by incoming cosmic rays. The initial density and temperature fields are set to be uniform and equal to unity. The initial internal energy $e=C_v T$ defines the initial rms Mach number; we take it equal to 0.23 with local values up to 0.9. The Prandtl number is unity and the adiabatic index is $\gamma=1.4$. The Reynolds number, based on the rms velocity and the integral scale, is $\mathrm{Re}=700$ with a viscosity such that $1/\nu=20\,000$.

C. Two-dimensional dynamical evolutions

We now examine the numerical results for simulations with an initial ratio $\chi=0.1$. This ratio is stabilized around 0.03 at $\tau=100$ as shown in Fig. 1. The rms Mach number, initially equal to 0.23, has a quasiconstant value during its time evolution, with a decrease of the order of 1% at the final time $\tau=200$, as shown on the right-hand side of Fig. 1. However, the maximum of the local Mach number, initially equal

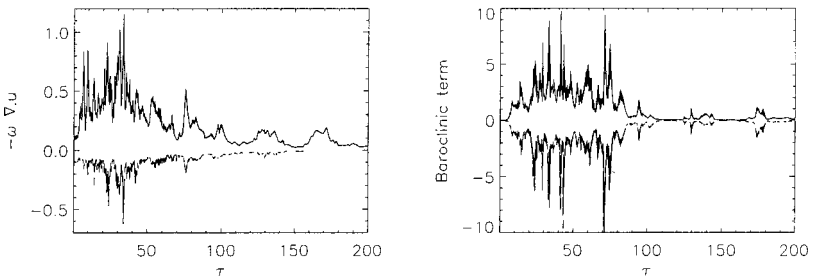

FIG. 6. Temporal evolution of the maximum and minimum of the vorticity production terms; left: $-\omega\nabla\cdot\mathbf{u}(\tau)$; right: the baroclinic term $\nabla\rho\times\nabla p/\rho^2(\tau)$.

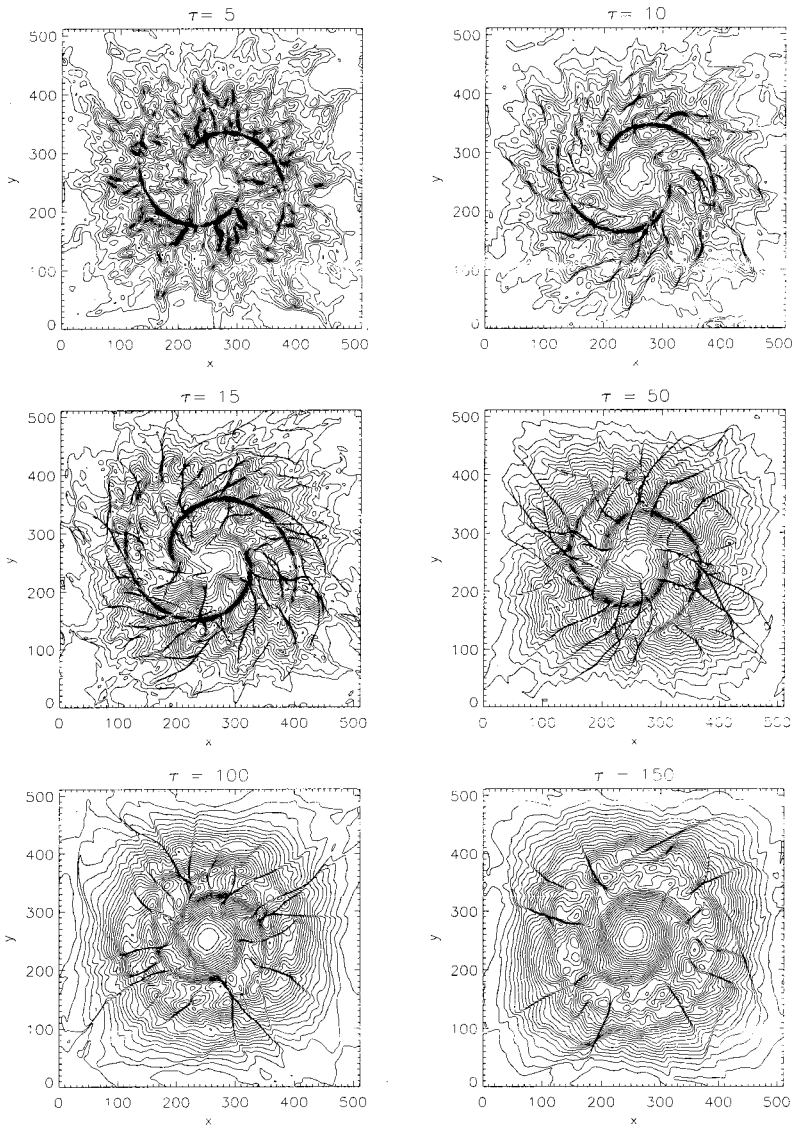

FIG. 7. Map of the total velocity square as a function of time for time ranging from $\tau=5$ to $\tau=150\sim 3\tau_{ac}$. The maximum values of velocity square $\mathbf{u}^2$ are, respectively, 1.23×10^{-2}, 1.08×10^{-2}, 8.02×10^{-3}, 7.11×10^{-3}, 5.89×10^{-3}, 4.48×10^{-3} at times 5, 10, 15, 50, 100, 150.

to 0.9, decreases along the simulation and stabilizes itself around 0.55 at a time around $\tau=100$. Note that it takes a sound wave a time $\tau_{ac}=2\pi/c_{rms}\sim47$ to cross the computational box of size $L=2\pi$; this time is the characteristic compressible time for the interaction of a sound wave with the central spiral vortex.

All along the dynamical evolution of the two-dimensional flow, the wave numbers of the compressible square velocity, when compared to the incompressible ones, are dominant at small scales ($k>5$) while they are subdominant at large scales (Fig. 2), as observed in numerous numerical simulations using, for example, random initial conditions.[17] Hence, when integrated over wave numbers, this leads to an incompressible square velocity remaining larger than its compressible counterpart (see Fig. 3), as well as to a ratio χ decreasing from its initial value of 0.1 (Fig. 1). One can distinguish three different regimes on the temporal evolution of the enstrophy $\Omega^s(\tau)=\frac{1}{2}\langle(\boldsymbol{\omega})^2\rangle$ and of its compressible counterpart, the square velocity divergence $\Omega^d(\tau)=\frac{1}{2}\langle(\boldsymbol{\nabla}\cdot\mathbf{u})^2\rangle$ (Fig. 4). The first one, extending from $\tau=0$ to $\tau\sim50$, corresponds to an acoustic time and starts with the rapid generation of weak shocks up to $\tau\sim15$, followed by a decrease of $\Omega^d(\tau)$ up to $\tau\sim50$ during an interaction time between the spiral vortex and the sound waves. This behavior is also visible on the temporal evolution of the ratio of maximal to minimal mass density $\rho_{max}(\tau)/\rho_{min}(\tau)$ which is characteristic of the flow compressibility, because of the aggregation and condensation on the one hand, and rarefaction waves on the other hand (Fig. 5 at the left-hand side). During this phase, there is no creation of enstrophy; $\Omega^s(\tau)$ decays rapidly from $\tau=0$ to $\tau\sim15$, displaying then a small plateau (from $\tau\sim15$ to $\tau\sim40$). This is similar to the incompressible case: all the incompressible small scales are initially present for the incompressible part of the initial velocity which is a solution of the incompressible equations; thus enstrophy can only decrease through dissipation. Moreover, the compressible modes of the velocity do not produce any substantial enstrophy at large scales, as they are mostly prevalent at small scales. However, the interactions between the incompressible and compressible modes are very intense as shown on the temporal evolution of the maxima and minima of the nonlinear terms of the vorticity equation (Fig. 6); up to $\tau\sim50$ for the $-\omega\boldsymbol{\nabla}\cdot\mathbf{u}$ term, and up to $\tau\sim80$ for the baroclinic term $\boldsymbol{\nabla}\rho\times\boldsymbol{\nabla}p/\rho^2$.

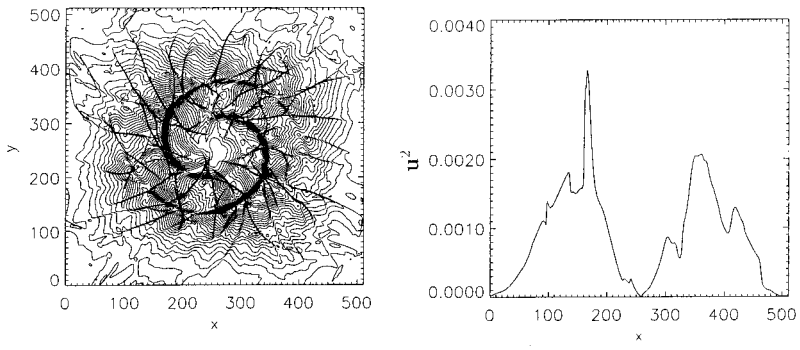

FIG. 8. Velocity square contours and its profile at $y=256$ at time $\tau=30\sim0.60\tau_{ac}$. The maximum values of velocity square $\mathbf{u}^2$ is 7.41×10^{-3}.

Note that the ratio $\chi(\tau)$ (Fig. 1, on the left-hand side) and the compressible square velocity $E^d(\tau)=\langle(\mathbf{u}^d)^2\rangle$ (Fig. 3, on the right-hand side) present altogether a similar behavior: a rapid increase up to $\tau\sim10$, followed by a decrease which saturates from $\tau\sim15$ to $\tau\sim40$.

The second temporal regime, from $\tau\sim50$ to $\tau\sim100$, corresponds to a second interaction of the weak shocks with the central spiral vortex, and with other weak shocks created simultaneously. The weak shocks dissipate less energy, since most of it has already been dissipated at small scales, as visible on the slowing down of the decrease of $\Omega^d(\tau)$ (Fig. 4), measuring the viscous dissipation of the kinetic compressible energy, to within a pressure term. The fluctuations of the ratio $\rho_{max}(\tau)/\rho_{min}(\tau)$ (Fig. 5) stabilize around 1.9 with short weak oscillations. They reveal the presence of small turbulent fluctuations of the compressible velocity that have not yet dissipated.

The third regime, from $\tau\sim100$ onward, is an acoustic one, during which the compressible velocity fluctuations travel through the computational box, with almost no sizable interactions with the incompressible part. This is visible on the strong diminution of the maximum and the minimum of the vorticity production terms (Fig. 6). The ratios $\rho_{max}(\tau)/\rho_{min}(\tau)$, $\chi(\tau)$ and $E^d(\tau)$ are quasiconstant, with values, respectively, oscillating around 1.5, 0.03, and 0.001.

We now turn to the dynamics of the flow in physical space. We show the square velocity as a function of time in Fig. 7, from $\tau=5$ to $\tau=150$, corresponding approximately to three acoustic times.

The intense fine compressible structures are weak shocks which interact strongly with the spiral branches of the vortex during a characteristic time comparable to the acoustic time. One can observe these interactions on the iso-contours of the velocity square (Fig. 7); note as well the persistence of the spiral structure of the solenoidal component of the velocity, even though the maximum initial Mach number is close to unity. This is due to the fact that the energetic structures of the compressible velocity are at smaller scales than the characteristic scale of the spiral arms. The energetic structures of the square velocity field are exemplified by plotting a profile (Fig. 8, on the right-hand side) of the field at time $\tau=30\sim0.6\tau_{ac}$ (Fig. 8, on the left). In fact, the most intense shocks are localized along the branches of the spiral vortex, as visible on the profiles plotted in Fig. 9 for, respectively, the vorticity field (Fig. 10, on the left-hand side) and the velocity divergence field (Fig. 10, on the right-hand side) shown at time $\tau=30\sim0.6\tau_{ac}$. Moreover, these compressible structures locally—in the vicinity of the spiral arms—are perpendicular to them, leading globally to what can be called an ''ortho-spiral'' structure; the divergence field is locally perpendicular to the vorticity and is then carried along in the global rotation of the flow enticed by the strong vortex; hence, the complex structure for $\nabla\cdot\mathbf{u}$ whose skeleton is the spiral of vorticity.

D. Three-dimensional spectral properties

In this section, we compute numerically the three-dimensional spectrum of the compressible square velocity from the two-dimensional spectra of the square velocity divergence according to relation (40), as well as its incompressible counterpart from the two-dimensional enstrophy spectra.[8] The three-dimensional spectra are obtained through a temporal integration of the two-dimensional ones; the upper time limit of this integration, τ_{cut}, is chosen according to the dynamical evolution of the two-dimensional flow.

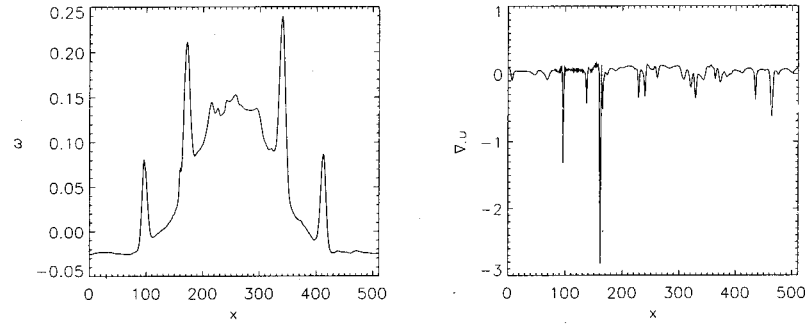

FIG. 9. Profiles at $y=256$ of vorticity (left) and $\nabla\cdot\mathbf{u}$ (right) at time $\tau=30\sim0.60\tau_{ac}$.

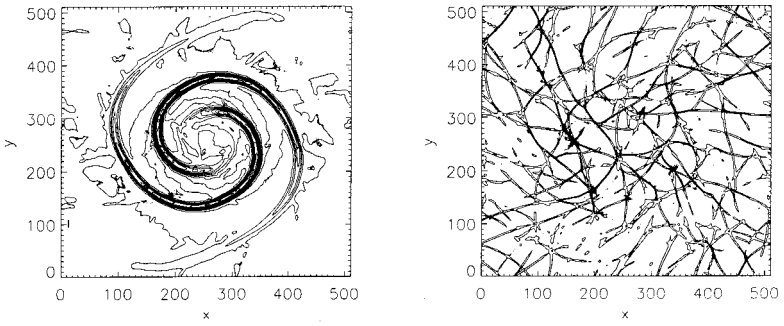

FIG. 10. At time $\tau=30\sim0.60\tau_{ac}$, contour plot of the vorticity ω (left) with minimum and maximum values of -0.08 and 0.25, and, on the right, contours of $\nabla\cdot\mathbf{u}$ with values ranging from -3.68 up to 1.25.

For the compressible part of the flow, the temporal integration is carried up to $\tau^d_{cut}=50\sim\tau_{ac}$ to take into account only one interaction between the shocks and the vortex structure. In the model, after this time, the compressible structures, which have interacted with the spiral vortex, leave the influence domain of the local vortex; they travel away while weakening because of dissipation until another intense spiral vortex is encountered which re-energizes them again. During this travel between intense vortices, the compressible fluctuations are assumed to have nonrelevant contributions to the three-dimensional compressible kinetic spectrum.

The resulting compressible spectrum, compensated by a factor $k^{5/3}$, is plotted in Fig. 11 for different values of the external strain rate, namely $a=1$, $a=4$, and $a=10$; note that a higher value of the parameter a, that is related to an increase of the strain intensity, allows for an acceleration of the energy cascade mechanism from large to small scales. This procedure thus enables us to extend the range of the domain of the three-dimensional wave numbers toward higher values, from 1 to $S^{1/2}(\tau)\times k_{max}=\sqrt{1+a\tau}\times k_{max}$, where k_{max} is the highest wave number reached in the two-dimensional numerical simulation, with $k_{max}=256$ here. For $a=1$, a $k^{-5/3}$ inertial range is obtained and extends roughly from $k=35$ to $k=70$. For $a=4$ and $a=10$, this $k^{-5/3}$ range extends from $k=70$ to $k=130$ and $k=110$ to $k=210$, respectively. Thus, the increase of the strain rate enlarges the $k^{-5/3}$ range of the spectrum, without a significant change of the spectral slope, thus clearly pointing out to the correlation between the $k^{-5/3}$ range and the strain intensity. This physical property could be due to a self-similar behavior of the square of the velocity divergence analogous to that of the enstrophy as shown by Lundgren[8] in the purely incompressible case. However, one has to realize that increasing a enables one to enlarge the inertial range, but does not change the total number of two-dimensional wave numbers used to construct the three-dimensional spectrum. Note that in the case of a substantially lower Mach number than that taken here, the 5/3 spectrum does not obtain; for example, for an initial rms Mach number of order 10^{-2}, with local maxima of the Mach number up to 3.9×10^{-2}, our model does not provide a well-defined self-similar range for the spectrum, probably due to the weak energy exchanges, in that case, between the compressible and incompressible velocity scales.

The three-dimensional incompressible velocity spectrum is computed from the the temporal integration of the two-dimensional enstrophy spectra, up to either $\tau^s_{cut}=50$ or $\tau^s_{cut}=100\sim2\tau_{ac}$; the second choice of τ^s_{cut} is done in order to check the influence of the temporal upper limit. Indeed, the lifetime of the spiral vortex is shorter than in the purely incompressible case; this can be interpreted as the result of the energy exchanges between the compressible and the incompressible flow components leading to the formation of inhomogeneities inside the spiral branches, thus reinforcing their dissipation. The temporal evolution of the intensity of these energetic exchanges, as can be observed in Fig. 6

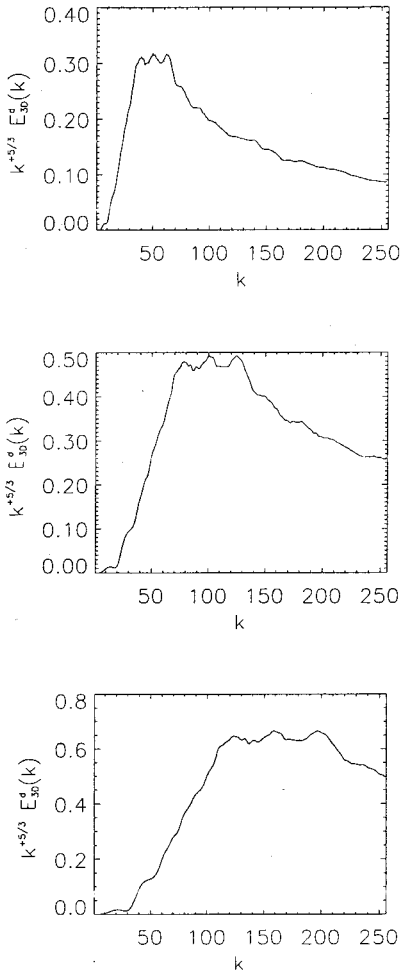

FIG. 11. Compressible three-dimensional compensated spectra obtained with a time integration between $\tau=0$ and $\tau^d_{cut}=50\sim\tau_{ac}$ for various external strain rates $a=1$, $a=4$, and $a=10$.

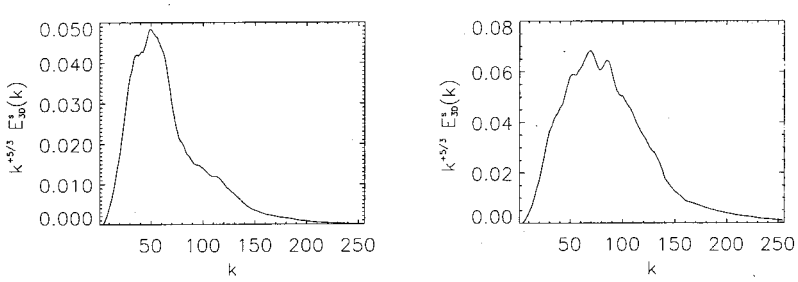

FIG. 12. Incompressible three-dimensional compensated spectra obtained with time integrations between $\tau_0=0$ and $\tau^s_{\text{cut}}=50$ (left), and $\tau^s_{\text{cut}}=100$ (right) for a unity external strain rate.

showing the vorticity production terms, leads to the choice of the values for τ^s_{cut} used to perform the temporal integration providing the incompressible spectrum. In fact, after $\tau \sim 100$, the spiral branches of the Lundgren vortex have considerably faded out and, as discussed before, we have entered an acoustic regime unrelated to the present problem. The resulting compensated spectra are plotted in Fig. 12. They display a lesser agreement with a $k^{-5/3}$ behavior on a shorter range of wave numbers than in the case of an incompressible flow at the same Reynolds number.[8] However, at the same Mach number, one can obtain a better agreement and a more extended scaling zone for flows at higher Reynolds numbers.

In fact, the numerical simulations we performed have shown that when increasing the Mach number, the $k^{-5/3}$ spectral range is extended for the compressible spectrum, while, when increasing the Reynolds number, this range is extended for the incompressible spectrum. At the resolution considered here, some compromise has to be found. In this work, we make the choice to favor the compressible aspect in considering a range of Mach numbers approaching locally unity. This explains, in part, the shorter $k^{-5/3}$ range obtained for the incompressible spectrum.

On the other hand, one has to notice that the spectral decrease at small scale that we observe here can be compared with a similar behavior obtained by Lundgren[8] for the incompressible spectrum, when considering an initial condition consisting in an axisymmetric central vortex surrounded by eight identical smaller circular vortices. Such an initial condition is not a solution of the Navier–Stokes equations and the interactions among its different substructures feed all the scales, including the smallest ones. This could influence the self-similar behavior of the temporal decrease of the enstrophy, lead to the presence of inhomogeneities, and enforce the dissipation, thus explaining the observed spectral decrease on the compensated plots.

IV. CONCLUSION

We have extended the Lundgren spiral vortex model to compressible flows and shown that it is compatible with a $k^{-5/3}$ Kolmogorov scaling range for the spectrum of the compressible square velocity, as well as for the incompressible one, although with a lesser agreement on a shorter spectral extent for the latter. Such spectral scaling laws are observed in three-dimensional numerical simulations of either forced or decaying compressible turbulence, at rms Mach numbers of order unity.[9,10] Note that, although our simulations are at rms Mach numbers of 0.23, they display local values of the Mach numbers up to the order of unity.

The model is based on geometrical considerations linked to the roll-up of the velocity divergence fluctuations by the strong vorticity structures of the flow. We have thus shown the crucial role of the intense vorticity structures, including in the case of compressible flows. Indeed the $k^{-5/3}$ scaling law satisfied by the energy spectrum of the compressible velocity component could have as its origin the most intense vorticity structures which drive the compressible modes in a global roll-up motion. This differential roll-up of compressible fluctuations combined with a large scale straining could thus explain the $k^{-5/3}$ spectrum by a process similar to the one described by Gilbert[18] for incompressible flows. Indeed, one observes that the divergence of the velocity displays what can be called an ortho-spiral organization: the divergence field, locally perpendicular to the vorticity, is carried along in the global rotation of the flow enticed by the strong vortex; hence, the complex structure for $\boldsymbol{\nabla}\cdot\mathbf{u}$ leads as well to a 5/3 spectrum (to within intermittency corrections, which is a topic not considered by these types of models), and for the same basic reasons as exemplified in the model developed by Gilbert: it is a combination of stretching by a strain field and a differential rotation by a vorticity field which leads to such a balance.

[1]T. S. Lundgren, ''Strained spiral vortex model for turbulent fine structure,'' Phys. Fluids **25**, 2193 (1982).
[2]A. Kolmogorov, ''The local structure of turbulence in incompressible viscous fluid for very large Reynolds number,'' Dokl. Akad. Nauk SSSR **30**, 9 (1941).
[3]A. A. Townsend, ''On the fine scales structures of turbulence,'' Proc. R. Soc. London, Ser. A **208**, 534 (1951).
[4]S. Corrsin, ''Turbulent dissipation fluctuations,'' Phys. Fluids **5**, 1301 (1962).
[5]H. Tennekes, ''Simple model for the small-scale structure of turbulence,'' Phys. Fluids **11**, 669 (1967).
[6]D. I. Pullin and P. G. Saffman, ''On the Lundgren–Townsend model of turbulent fine scales,'' Phys. Fluids A **5**, 126 (1993).
[7]D. I. Pullin, J. D. Buntine, and P. G. Saffman, ''On the spectrum of a stretched spiral vortex,'' Phys. Fluids **6**, 3010 (1994).
[8]T. S. Lundgren, ''A small-scale turbulence model,'' Phys. Fluids A **5**, 1472 (1993).
[9]D. H. Porter, A. Pouquet, and P. R. Woodward, ''Kolmogorov-like spectra in decaying three-dimensional supersonic flows,'' Phys. Fluids **6**, 2133 (1994).
[10]D. H. Porter, A. Pouquet, and P. R. Woodward, ''Inertial range structures in decaying compressible turbulent flows,'' Phys. Fluids **10**, 237 (1998).
[11]P. Woodward and P. Colella, ''The numerical simulation of two-dimensional fluid flow with strong shocks,'' J. Comput. Phys. **54**, 115 (1984).
[12]D. H. Porter, A. Pouquet, and P. R. Woodward, ''Compressible flows and

vortex stretching. Small-scale structures,'' in *Three-dimensional Hydrodynamics and Magnetohydrodynamics Turbulence*, edited by M. Meneguzzi, A. Pouquet, and P. L. Sulem [Lect. Notes Phys. **462** 51 (1995)].
[13]T. Gomez, ''Dynamique des structures *à* petites échelles en écoulements turbulents compressibles ou MHD: Modélisation et intermittence,'' thesis, University of Paris 6, 1999.
[14]J. D. Gibbon, A. S. Fokas, and C. R. Doering, ''Dynamically stretched vortices as solutions of the 3D Navier–Stokes equations,'' Physica D **132**, 497 (1998).
[15]D. I. Pullin, ''Pressure spectra for vortex models of fine-scale homogeneous turbulence,'' Phys. Fluids **7**, 849 (1995).
[16]J. E. Moyal, ''The spectra of turbulence in a compressible fluid; Eddy turbulence and random noise,'' Proc. Cambridge Philos. Soc. **48**, 329 (1951).
[17]T. Passot and A. Pouquet, ''Compressible turbulence with a perfect gas law: A numerical approach,'' J. Fluid Mech. **181**, 441 (1987).
[18]A. Gilbert, ''A cascade interpretation of Lundgren's strectched spiral vortex model for turbulent fine structure,'' Phys. Fluids A **5**, 2831 (1993).